J Comput Aided Mol Des (2009) 23:677–689
DOI 10.1007/s10822-009-9295-y

Modeling of peptides containing D-amino acids: implications on cyclization

Austin B. Yongye · Yangmei Li · Marc A. Giulianotti · Yongping Yu · Richard A. Houghten · Karina Martínez-Mayorga

Received: 6 March 2009 / Accepted: 25 June 2009 / Published online: 11 July 2009

Abstract Cyclic peptides are therapeutically attractive due to their high bioavailability, potential selectivity, and scaffold novelty. Furthermore, the presence of D-residues induces conformational preferences not followed by peptides consisting of naturally abundant L-residues. Therefore, comprehending how amino acids induce turns in peptides, subsequently facilitating cyclization, is significant in peptide design. Here, we performed 20-ns explicit-solvent molecular dynamics simulations for three diastereomeric peptides with stereochemistries: *LLLLL*, *LLLDL*, and *LDLDL*. Experimentally *LLLLL* and *LDLDL* readily cyclize, whereas *LLLDL* cyclizes in low yield. Simulations at 310 K produced conformations with inter-terminal hydrogen bonds that correlated qualitatively with the experimental cyclization trend. Energies obtained for representative structures from quantum chemical (B3LYP/PCM/cc-pVTZ//HF/6-31G*) calculations predicted pseudo-cyclic and extended conformations as the most stable for *LLLLL* and *LLLDL*, respectively, in agreement with the experimental data. In contrast, the most stable conformer predicted for peptide *LDLDL* was not a pseudo-cyclic structure. Moreover, D-residues preferred the experimentally less populated α_L rotamers even when simulations were performed at a higher temperature and with strategically selected starting conformations. Energies calculated with molecular mechanics were consistent only with peptide *LLLLL*. Thus, the conformational preferences obtained for the all L-amino acid peptide were in agreement with the experimental observations. Moreover, refinement of the force field is expected to provide far-reaching conformational sampling of peptides containing D-residues to further develop force field-based conformational-searching methods.

Keywords Peptide conformation · Force field · Quantum mechanics · Molecular dynamics simulations

Introduction

Cyclic peptides are distributed naturally in bacteria, plants and animals, but not in humans [1]. They display potential therapeutic properties such as: moderating angiogenesis [2], trypsin inhibition and cancer prevention [3], anti-HIV cellular [4, 5] and anti-adenoviral [6] activities. The cyclization of a peptide can occur through side-chain to side-chain [2, 7], head to tail [3], or side-chain to main chain connectivity [2, 7]. Cyclization confers resistance to proteolysis [8] subsequently increasing the bioavailability of therapeutic peptides. In addition, cyclization invariably restricts a peptide's conformational degrees of freedom, thereby facilitating the determination of its biologically active conformers [7]. The restricted conformation also suggests that cyclic peptides can only be accommodated in a limited number of binding or active sites imparting increased selectivity towards receptors [7, 9]. It has been suggested that the increase in the rigidity of peptides upon cyclization provides an opportunity for their exploration as structural scaffolds in drug design [10]. For these reasons, natural and

Electronic supplementary material The online version of this article (doi:10.1007/s10822-009-9295-y) contains supplementary material, which is available to authorized users.

A. B. Yongye · Y. Li · M. A. Giulianotti · R. A. Houghten · K. Martínez-Mayorga (✉)
Torrey Pines Institute for Molecular Studies, Port Saint Lucie, FL 34987, USA
e-mail: kmartinez@tpims.org

Y. Yu
College of Pharmaceutical Science, Zhejiang University, Zijin Campus, Hangzhou 310058, People's Republic of China

synthetic cyclic peptides are actively investigated for the design of combinatorial libraries of compounds with potential therapeutic properties.

Over the past 20 + years our research group has been involved in peptide synthesis, and has successfully optimized the experimental conditions for the synthesis and biological evaluation of combinatorial peptide libraries [11, 12]. The therapeutic properties of cyclic peptides prompted us to explore them as potential lead compounds. A common strategy employed to improve yields in cyclization reactions involves the incorporation of amino acid residues such as proline, glycine, *N*-alkylated and D-amino acids, which induce turns in the conformations of peptides [13–15]. It is a general observation that the cyclization of linear peptides that do not contain turn structure-inducing residues is improbable or a very slow process. However, successful cyclization reactions have been possible for thymopentin-derived pentapeptides and it was observed that the cyclization is favored by *C*-terminal D-amino acids.[16] Given that an amino acid residue influences the rotamer preferences of its neighbors [17, 18], one consideration in the synthesis includes the number of turn-inducing residues to incorporate. Moreover, individual amino acid residues in a peptide may exist in several quadrants of the Ramachandran plot, posing a significant challenge in assessing the synergistic effects of these turn-inducing amino acids on the overall conformation of a given peptide. Experimental [18] and theoretical [18, 19] studies have shown that the positions of amino acid residues in a sequence are crucial in determining the overall folds of peptides. Therefore, another consideration in designing libraries of cyclic peptides is which positions in the peptide are optimal for the turn-inducing residues. Consequently, understanding the conformational properties of amino acids, which induce turns in peptides thereby facilitating peptide cyclization, should aid the rational design and synthesis of cyclic peptides.

Molecular dynamics (MD) simulations are one approach to elucidate the conformational properties of peptides. They have been employed extensively to provide atomic level insights about the folding behavior of peptides [19–23]. It has been pointed out that the factors that influence the ability of a precursor to cyclize are: Steric hindrance to ring closure, kinetic competition with the dimerization reaction, and the energy from the transition-state to the reaction product (cyclic peptide). [24]. Methodologies to predict the tendencies of peptides to undergo cyclization have been reported. [24, 25] Based on molecular mechanics calculations and experimental evidence involving cyclotetrapeptides, Cavelier-Frontin et al. [24] concluded that the determining factor for ring closure is the transition-state energy, wherein those peptides that are able to have transition-states in a low strain conformation have more chances to undergo cyclization. In a subsequent study Besser et al. [24, 25] developed a methodology based on the structural comparison between the conformations of the linear precursor and the conformation in the transition-state. Their first assumption was that the cyclization tendency was correlated with the relative probability of being found in a cyclization-prone conformation of the backbone, and concluded that the conformational space of the linear analogs should be considered in the calculation of the cyclization tendencies. It should be noted that in order to compare the results from MD simulations with experimental observables, the ergodicity hypothesis needs to be fulfilled. The generation of enough representative conformations of the system highly depends on the simulation time scale, molecular mechanics (MM) force field and temperature employed, among other features. Nonetheless, there are examples of MD simulations that correctly predict the native folds of peptides [22, 26]. Utilizing MD simulations Terada et al. [19] were able to delineate specific amino acid residues in a decapeptide, which were required for the peptide to achieve a β-hairpin structure. In addition, Krautler et al. [20] successfully predicted the structure of a hairpin through MD simulations. Therefore, by employing robust biomolecular force fields, appropriate solvent models and vigorous simulation protocols, MD simulations have predicted reasonably well the conformational properties of peptides.

In an effort to increase our understanding of peptide cyclization, here we sought to reproduce and elucidate, via explicit solvent MD simulations, the cyclization propensities of selected pentapeptides containing D-residues. We aim to employ molecular simulations in a predictive capacity by determining the cyclization propensities of peptide sequences to aid in the chemical synthesis of combinatorial libraries of this promising source of drug-like compounds.

Methods

Computational details

A structural model for the Asp-Leu-Thr-Phe-Gly-SBzl pentapeptide was generated from the Asp-Leu-Thr-Phe-Gly sequence, with all the *C*α atoms in the *L*-stereochemistry and in the α_R-helix conformation employing the "Build structure" tool of the Chimera program [27]. The Maestro version 8.5 graphical user interface (GUI), Schrodinger, LLC, was utilized to modify the chirality of the Cα atoms of Leu2 and Phe4, to generate the Asp-Leu-Thr-D-Phe-Gly and Asp-D-Leu-Thr-D-Phe-Gly peptides. The topology of the nonstandard thiobenzyl glycine residue was constructed by combining the pre-existing topologies of glycine, methane thiol and benzene fragments, while valence and dihedral angle parameters involving the thiobenzyl moiety were

incorporated from the pre-existing par_all27_prot_na_lipids_full.inp CHARMM parameter file. The standard residues were modeled employing the par_all27_prot_lipid.inp parameter set [28]. To be consistent with the experimental protonation states, the Asp residue was treated as the neutral species: deprotonated and protonated amine and carboxyl groups, respectively. Thus, the final peptides employed were neutral H-Asp-Leu-Thr-Phe-Gly-SBzl (**a**), H-Asp-Leu-Thr-D-Phe-Gly-SBzl (**b**) and H-Asp-D-Leu-Thr-D-Phe-Gly-SBzl (**c**).

Peptides "**a**," "**b**" and "**c**" were imported into the GUI of the visual molecular dynamics (VMD) program [29]. Each peptide was immersed in a pre-equilibrated box of the TIP3P [30] water model employing the Solvate plugin of VMD. A distance of 13 Å separated the edges of the boxes from the peptides, giving rise to 1,763, 1,734 and 1,603 water molecules solvating peptides "**a**," "**b**" and "**c**," respectively, with final box dimensions of $44 \times 43 \times 39$, $41 \times 46 \times 37$ and $42 \times 45 \times 35$, respectively. The NAMD2 program [31] was utilized for all energy minimizations and MD simulations performed with IBM p655 32 8-CPU Power4 node clusters at the University of Georgia, Athens, GA. Initially, the atomic positions of each system were optimized through 10,000 steps employing the conjugate gradient algorithm, under the constant volume-temperature ensemble. Next, the system was heated for 50 ps, under constant volume, by raising the temperature from 0 to 310 K in increments of 10 K/ps. Each system was equilibrated further at 310 K for 500 ps under isobaric-isothermal (NPT) conditions. The systems were next subjected to 20 ns of production dynamics under the NPT ensemble. At every stage non-bonded interaction cut-off and switch distances of 12.0 and 8.0 Å, respectively, were employed. Long-range electrostatic interactions were computed employing the particle-mesh Ewald summation method [32]. A time-step of 2 fs was employed to integrate Newton's equations of motion, while bonds involving hydrogen atoms were constrained at their equilibrium positions using the SHAKE algorithm during the MD simulations. Snapshots of the trajectory were collected every picosecond. Peptide backbone dihedral angles (ψ, φ), hydrogen bond interactions and inter-atomic distances were extracted from the trajectories utilizing the ptraj stand-alone program. The angle (donor-hydrogen-acceptor) and distance (donor–acceptor) cut-offs were 120° and 3.5 Å, respectively, for determining the occurrence of a hydrogen bond. The number of times a group of donor-hydrogen-acceptor atoms satisfied these constraints over the length of the simulation gave rise to the occupancy of the hydrogen bond. The trajectories were clustered with the g_cluster tool of GROMACS 4.0 [33]. The energies of all conformers within a cluster were computed utilizing the NAMDEnergy plug-in tool of VMD. In addition, partial quantum mechanics (QM) optimizations were performed on the representative structures from each cluster at the HF/6-31G* level of theory by constraining the (φ, ψ) dihedral angles at their MD-determined values. The corresponding single point energies were determined at the B3LYP/cc-pVTZ level of theory employing the polarizable continuum model (PCM) [34], with Gaussian 03 [35] at the high-performance supercomputing facility at Florida State University, Tallahassee, FL on Dell PowerEdge SC1435 compute nodes.

Synthesis of peptide thioesters and their related cyclic peptides

Detailed description of the chemical synthesis of the peptides studied here is described elsewhere [36, 37]. Briefly, peptide thioesters were prepared by solid-phase peptide synthesis (SPPS) using mercapto-methyl-phenyl silica gel as "volatilizable" support [36]. Boc amino acids (4 equiv) pre-activated for 5 min with PyBOP (4 equiv) and DIEA (6 equiv) in DMF were added to the mercapto-methyl-phenyl-functionalized silica gel and shaken at room temperature overnight. After washing with DMF, the Boc group was removed with 55% TFA in DCM to yield the resin bound peptide thioester. Stepwise peptide synthesis was carried out using a standard PyBOP/DIEA coupling protocol. After peptide chain elongation, the resin bound peptide was treated with anhydrous HF for 2 h at 0 °C. Following evaporation of the anhydrous HF with a gaseous nitrogen stream, the unprotected linear peptide thioester was obtained. To make the cyclic peptide, linear peptide thioesters were dissolved in a mixture of acetonitrile and 1.5 M aqueous imidazole solution with a volume ratio of 7:1 at a concentration of 1 mM. The reaction was allowed to proceed at 37 °C for 72 h and then quenched with 15% TFA in water. The reaction mixture was analyzed by LC-MS. The percent yields of the cyclic peptides obtained from the cyclization step are shown in Table 1.

As observed before, [38] the rotation of the starting sequence of a linear peptide affects the yields of cyclization. In our experiments, for instance, for peptide "a" (Asp-Leu-Thr-Phe-Gly-SBz), four peptide thioesters were synthesized following the rotating sequence to Leu-Thr-Phe-Gly-Asp-

Table 1 Cyclization in aqueous organic solvent

Linear Conformation	Cyclic[a] (%)	Dimer[a] (%)	Hydrolysis[a] (%)
L–L–L–L–L (a)	95	0	5
L–L–L–D–L (b)	5	21	74
L–D–L–D–L (c)	78	2	20

[a] Product yields(in percent) were determined by the peak area of HPLC at 214 nm

SBz, Thr-Phe-Gly-Asp-Leu-SBz, Phe-Gly-Asp-Leu-Thr-SBz, and Gly-Asp-Leu-Thr-Phe-SBz, respectively. Cyclization was then carried out under the conditions mentioned above. After 3 days of reaction, only two peptide thioesters, sequence Asp-Leu-Thr-Phe-Gly-SBz and Leu-Thr-Phe-Gly-Asp-SBz, completed the cyclization. The other three peptide thioesters remained mostly unaltered. The results clearly disclosed that changing positions of amino acids affects the fold of peptides, and in turn, affects the cyclization efficiency. The determination of the experimental conditions for the direct aminolysis of peptide thioesters in aqueous organic solvent included the effect of the solvent, the *C*-terminal amino acid, the *N*-terminal amino acid, stereochemistry, regioselectivity, and ring size. [37] Since the difference in reactivity to cyclization was remarkable among the stereoisomers synthesized we decided to rationalize via MD simulations the cyclization trends due to different stereoisomers based on structural and energetic considerations.

Results and discussion

In order to provide a structural interpretation of the observed tendencies of peptides H-Asp-Leu-Thr-Phe-Gly-SBzl (**a**), H-Asp-Leu-Thr-D-Phe-Gly-SBzl (**b**) and H-Asp-D-Leu-Thr-D-Phe-Gly-SBzl (**c**) to undergo cyclization, their conformational properties were investigated via explicit-solvent MD simulations.

Peptides "**a**" and "**b**" differ in the stereochemistry of the $C\alpha$ atom of Phe4; "**a**" and "**c**" are diastereomers with opposite stereochemistries at the $C\alpha$ atoms of Leu2 and Phe4. During experimental synthesis, peptides "**a**" and "**c**" underwent cyclization in water, while "**b**" did not. Initially, the peptides were minimized with their surrounding solvent medium, followed by gentle heating during which the temperatures of the systems were raised from 0 to 310 K in 10 K/ps increments. The systems were further equilibrated for 500 ps, followed by 20 ns of production dynamics at 310 K. The conformational flexibility of each peptide was explored via the time evolution of backbone RMSDs and dihedral angles. Intramolecular hydrogen bonds were employed to assess the degree of inter-terminal interactions. The trajectories were clustered to differentiate conformational families. Finally, the relative energies of the clusters and representative members of each cluster were computed molecular mechanically and quantum mechanically, respectively, to rationalize the experimental cyclization tendencies.

RMSD and (φ, ψ) conformational properties

The RMSD values fluctuated within a range of 0–2.0 Å for peptide "**a**," and from 0 to 3.0 Å for peptides "**b**," and "**c**," Fig. 1.

The variations observed in the RMSD values reflected differences in conformational behavior among the peptides with respect to the first frame in each simulation. A more detailed assessment of the conformational flexibility of each peptide was performed by analyzing the (φ, ψ) dihedral angles (see Scheme 1) sampled over the course of the MD simulations.

In general, and as expected from the distribution of backbone dihedral angles in a Ramachandran diagram, the ψ-angle exhibited more rotamer distributions with respect to the φ-angle, Fig. 2.

This is exemplified by comparing the rotamers of the (φ, ψ) angles of residues Leu2 and Phe4 in peptide "**a**," and the Leu2 residue of peptide "**b**," Fig. 2A, B, respectively. It was also observed that Asp1, Leu2, Thr3 and Gly5 sampled similar rotamers in peptides "**a**" and "**b**," (c.f. Fig. 2A, B). However, in contrast to the L-Phe4 residue in peptide "**a**" the D-Phe4 residue in peptide "**b**" did not undergo rotameric transitions, and only sampled (φ, ψ) values of ($87 \pm 13.1°$, $41 \pm 20.6°$) during the entire simulation. Note that for peptide "**c**" there were no significant variations in the (φ, ψ) angles of the internal residues: Leu2, Thr3, and Phe4. Reasons for this observation will be presented later in the manuscript. The trajectory of peptide "**a**" also revealed synchronized transitions among the ψ-angles of Leu2 and Phe4. During the first 2 ns the ψ-angles of Leu2 and Phe4 in peptide "**a**" oscillated about the eclipsed rotamer with values of $5 \pm 15.7°$ and $5 \pm 17.1°$, respectively. Between 2.5 and

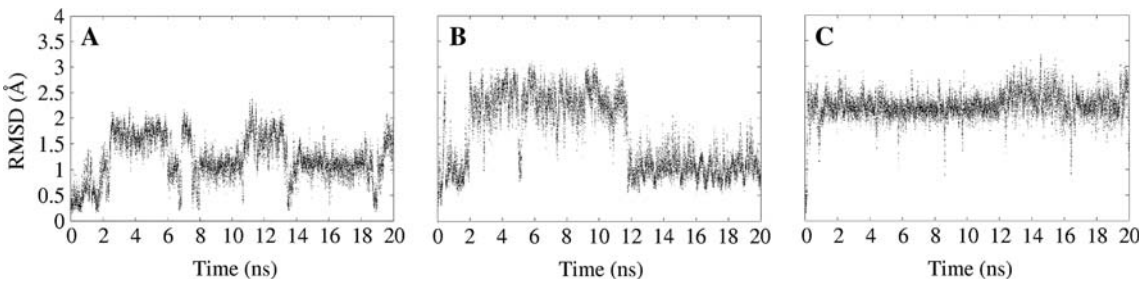

Fig. 1 RMSDs of the trajectories of peptides "**a**," "**b**," and "**c**" presented in **A**, **B**, and **C**, respectively

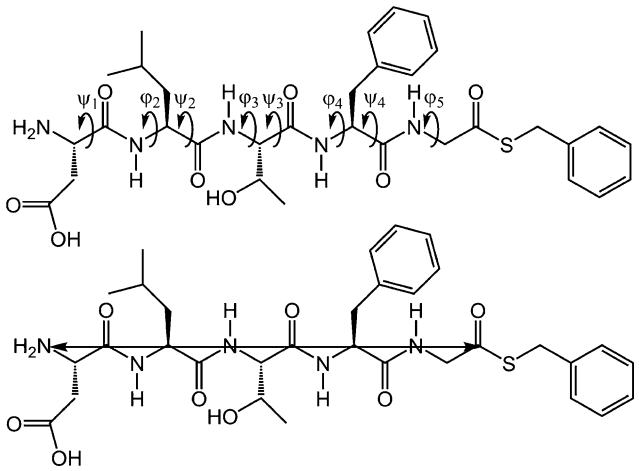

Scheme 1 Schematic representation of one of the pentapeptides employed in the molecular dynamics simulation. *Top* (φ, ψ) angles. *Bottom* End-to-end distance, defined by the N-terminal nitrogen atom and the C-terminal carbonyl carbon atom, is denoted by the arrow

6 ns they both effected simultaneous transitions to the *anti* rotamer, oscillating at approximately 140 ± 17.2° and 146 ± 46.3°, respectively, before returning to the eclipsed conformation.

Figure 2c portrays the (φ, ψ) trajectories of peptide "**c**" over the course of the MD simulation. The D-Leu2 residue exclusively populated +*gauche* + *gauche* (φ, ψ) values of (87 ± 14.7°, 44 ± 15.7°). Compared to the corresponding residue in peptides "**a**" and "**b**," this suggested a change in the flexibility of Leu2 from highly flexible to a well localized conformation when the amino acid was changed from the L to the D isomer. It should be noted that rotameric states with (φ, ψ) values of (∼87, ∼44°) were observed for all the residues with D-configuration: Phe4 in peptide "**b**," and Leu2 and Phe4 in peptide "**c**." The effects of D-amino acids on the local and overall conformational preferences of peptides have been investigated [17, 21, 39, 40]. A statistical analysis [17] of peptides in the Protein Data Bank containing D-amino acids indicated that these residues typically populated two regions of the Ramachandran diagram centered approximately at (120°, −135°) and (60°, 45°). The (φ, ψ) rotamers of (87 ± 13.1°, 41 ± 20.6°) adopted by D-Phe4 in peptide "**b**," (87 ± 14.7°, 44 ± 15.7°) and (89 ± 13.9°, 41 ± 22.8°) by the D-Leu2 and D-Phe4 residues, respectively, in peptide "**c**," would be consistent with the region of the Ramachandran diagram centered at (60°, 45°). The origin of this

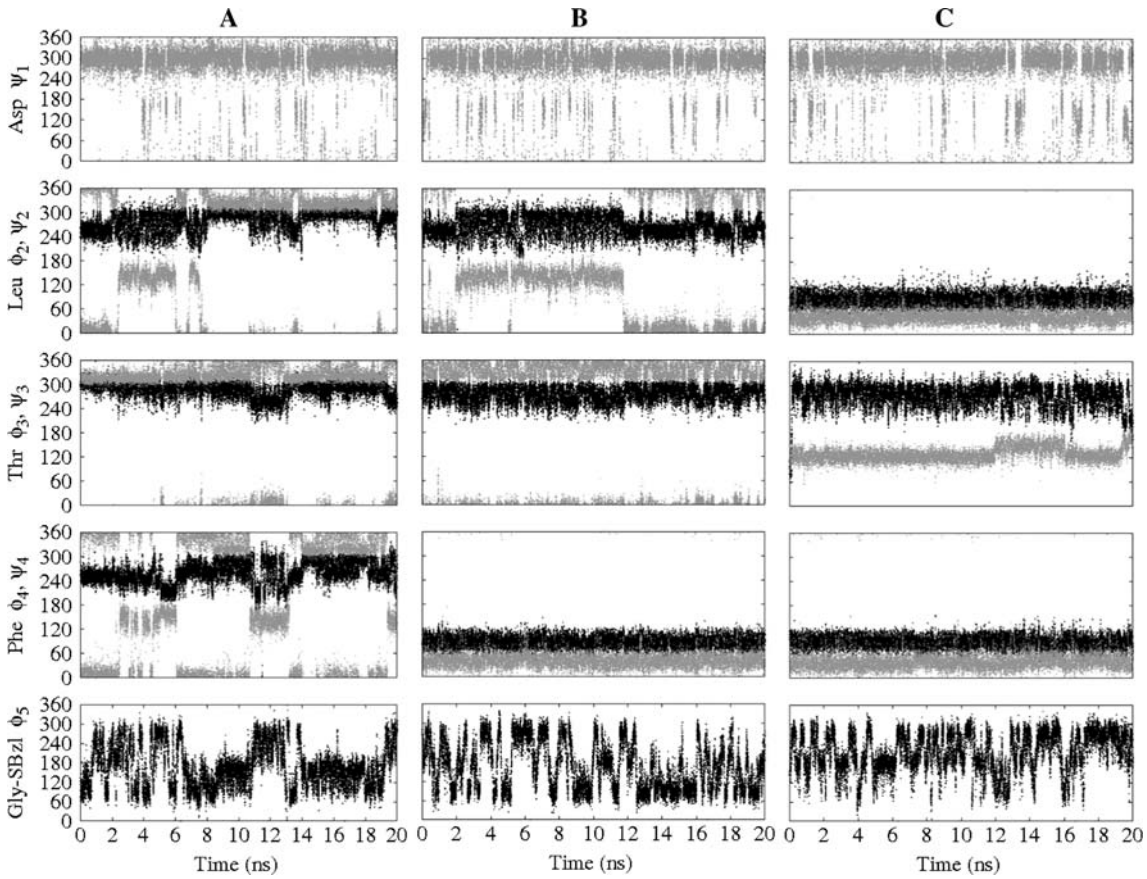

Fig. 2 Evolution of the (φ, ψ) angles of peptides "**a**", "**b**" and "**c**", **A**, **B**, and **C**, respectively. φ = *black*; ψ = *gray*. The corresponding residue is indicated in the *Y*-axis

different conformational behavior between L- and D-amino acids has not been clearly established. A series of factors such as steric, conformational entropy, amino acid side chain, stereochemistry, hydrophobic effect, solvent environment, local backbone dipole interactions and all other non-neighbor electrostatic interactions have been reported to contribute to the conformational preferences of peptide secondary structures [39, 41]. When structural models were built from peptide "**a**," and the D-stereochemistry included at Phe4 as in peptide "**b**," as well as at Leu2 and Phe4 for peptide "**c**," steric clashes were not apparent. Therefore, for peptides "**b**" and "**c**" unfavorable contacts originating from van der Waals interactions could not be the source of the rotamer distributions. Presumably, local backbone dipole interactions are having a major contribution. Interestingly, the (φ, ψ) values of ($-87 \pm 29.4°$, $129 \pm 19.9°$) in Thr3 were observed only in peptide "**c**." These angles corresponded to the β-region of the Ramachandran plot. It has been observed that D-amino acids in peptides with the LDL local configuration can induce β-turns at positions i, $(i + 1)$, $(i + 2)$ and $(i + 3)$ [17]. Evidently, the presence of a D-Leu at position two in peptide "**c**" induced a β-turn conformation at Thr3. As expected, the terminal residues displayed greater conformational freedom. In particular, the φ-angle of Gly5 showed the larger fluctuations in the three peptides analyzed, compared to the ψ-angle of Asp1.

Inter-termini distance, hydrogen bond occupancies and propensity for cyclization

Fluctuations in the inter-termini distances (*N*-terminal nitrogen atom to *C*-terminal carbonyl carbon atom, Scheme 1), correlated with rotamer transitions in all the peptides. The inter-termini distances for the three peptides over the course of the simulations are presented in Fig. 3.

In peptide "**a**" during the first two nanoseconds, the ψ values of Leu2 and Phe4 were $5 \pm 15.7°$ and $5 \pm 17.1°$, Fig. 2A, respectively, and the inter-termini distance oscillated between 6 and 8 Å, Fig. 3A. When the ψ angles flipped to their *anti* rotamers, from 2.5 to 6 ns, the inter-termini distance increased to within 10–14 Å, before returning to the 6–8 Å range when the ψ angles reverted to their eclipsed rotamers. In a third event, the ψ-angle of Phe4 sampled the *anti* rotamer between 11 and 13 ns, (Fig. 2A Phe4) resulting in a relatively moderate increase in the inter-termini distance to 8–10 Å. This transition was not accompanied by a corresponding transition in the ψ-angle of Leu2. For peptide "**b**" variations in the inter-termini distance, Fig. 3B, were mostly related to fluctuations in the ψ-angle of Leu2, Fig. 2B. The first two nanoseconds the ψ-angle fluctuated about $16 \pm 36.3°$, while the inter-termini distance was between 4 and 8 Å. From about 2–12 ns the ψ-angle made a transition and populated the $135 \pm 35°$ rotamer, which was accompanied by a corresponding lengthening of the inter-termini distance to 10–14 Å. In peptide "**c**" only the Gly5 terminal residues displayed significant rotamer transitions, Fig. 2C. However, these transitions had no apparent correlation with the inter-termini distance, Fig. 3C. The backbone dihedral angles of Asp1 and Thr3 sampled few rotamers and as such, had no significant impact on the inter-termini distance and in the propensity for cyclization.

In general, the conformational freedom of peptides and proteins in the unfolded structure contributes significantly to the overall stability of the system. This stability is attributable to the higher entropy (number of microstates) of the extended structure compared to the folded one; therefore the extended structure is generally preferred. [42] On the other hand, highly organized secondary structures are stabilized, among other factors, by several internal hydrogen bonds that contribute to the enthalpy term of the free energy equation. The pre-organization of the peptides studied here, that eventually lead to cyclization, were evaluated by the occurrence and population of internal hydrogen bonds between distant residues, such as $(i, i \pm 3)$ or $(i, i \pm 4)$. Hydrogen bond interactions were analyzed employing distance and angle cut-offs of 3.5 Å and 120°, respectively. Table 2 shows percent occupancies of hydrogen bonds in the three peptides for the particular ensembles of conformers produced for each simulation.

In peptide "**a**" hydrogen bonds between Asp1 (O)–Phe4 (N–H), Asp1 (O)–Gly5 (N–H) and Leu2 (O)–Gly5 (N–H) were present with occupancies of 24, 28 and 28%,

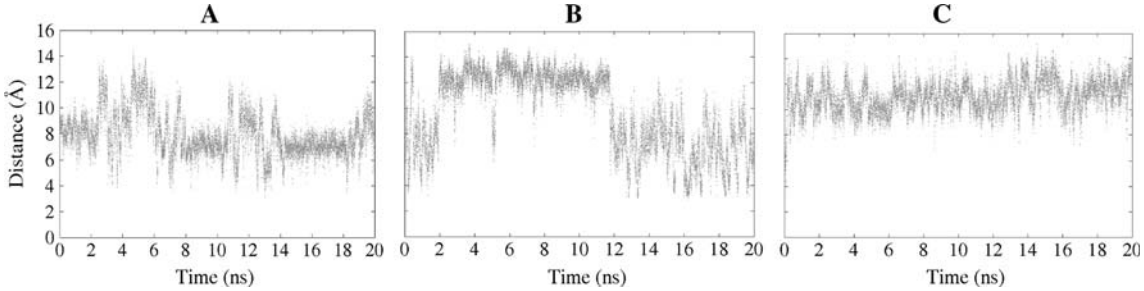

Fig. 3 The inter-termini distance (Asp N–Gly C) of peptides "**a**", "**b**" and "**c**", **A**, **B**, and **C**, respectively, during the MD simulation

Table 2 Hydrogen bond occupancies in the simulations with peptides "**a**," "**b**" and "**c**"

Hydrogen bonds	Occupancy (%)
Peptide "**a**"	
Asp1 (O)–Phe4 (N–H)	24
Asp1 (O)–Gly5 (N–H)	28
Leu2 (O)–Gly5 (N–H)	28
Peptide "**b**"	
Asp1 (O)–Phe4 (N–H)	4
Peptide "**c**"	
Leu2 (O)–Gly5 (N–H)	9

respectively, a good indication of the propensity for cyclization. In peptide "**b**" the (i, $i \pm 3$) hydrogen bond was formed between Asp1 (O)–Phe4 (N–H) with an occupancy of only 4%, whereas the occupancy of the (i, $i \pm 3$) hydrogen bond in peptide "**c**," Leu2 (O)–Gly5 (N–H) was 9%. The hydrogen bond occurrence and occupancies for peptides "**a**" and "**b**" agreed with the experimental cyclization observed: the most and least cyclized peptides, respectively. For peptide "**c**" the experimental yield of the cyclic monomer was 78%. The hydrogen bond occupancy of peptide "**c**" seemed to be less than expected. However, from the trajectories shown in Fig. 2C it was evident that the conformers populated was located in a deep energy minimum with no significant conformational transitions. The lack of conformational changes could be attributed to insufficient sampling or simulation time, or to the fact that peptide "**c**" can only be present in such specific rigid conformations. Since a greater percentage of hydrogen occupancies were expected for "**c**," the rigidity of all backbone angles indicated that more conformational sampling would be required to adequately represent peptide "**c**."

Conformational energy by means of quantum chemical calculations

As a final point, to identify global conformational families arising from the individual (φ, ψ) angles, the trajectories were clustered into conformational states, utilizing a 1.2-Å cut-off with the GROMOS algorithm of the GROMACS g_clustering tool. The representative structures from each cluster were selected and their energies computed at the B3LYP/PCM/cc-pVTZ//HF/6-31G* level of theory. During the optimization, the (φ, ψ) backbone dihedral angles were constrained at their solution-preferred rotamers, while the rest of the molecule was allowed to relax. It was hypothesized that peptides with high probabilities of undergoing cyclization would have low energy conformers with the terminal residues in close proximity. While for peptides that did not cyclize extended structures would be more stable. The QM and MM relative energies, as well as inter-terminal distances are presented in Table 3, while the representative structures identified from each trajectory and cluster are portrayed in Fig. 4.

For a qualitative comparison the clusters were partitioned into "curved", "transition", and "extended" backbone topologies. "Transition" topologies denoted conformations that were partially curved and extended at different segments of the peptide. Note that this "transition" topology does not refer to the transition-state geometry. The experimental data indicated that peptide "**a**" underwent cyclization. The QM relative energies, Table 3 and Fig. 4A, pointed to a curved backbone structure being the most stable, in agreement with the experimental observations. One of the other three "curved" structures identified, cluster1, displayed a significantly higher relative energy of 8.13 kcal/mol. This high energy might suggest the presence of unfavorable dipole interactions [41]. Notably, two other "curved" structures, from clusters 3 and 4, were comparably closer with relative energies of 1.49 and 2.12 kcal/mol, respectively. It should be noted that one "extended" conformer was less than 1 kcal/mol from the lowest energy structure. Representative structures identified from the trajectory of peptide "b" are shown in Fig. 4B. Among the three peptides, cyclization in peptide "b" was minor. Indeed, the relative energies showed the extended conformation as the most stable, Table 3. In peptide "c" the most stable conformer corresponded to an "extended" structure, Fig. 4C. The "curved" conformation, has been recognized as pre-requisite to be fulfilled in order to undergo cyclization [25]. Thus, molecules that are able to reach "curved" conformations have overcome the first conformational requirement for cyclization. Once the two termini have approached each other, additional rearrangements are needed in order to reach the transition-state. The full characterization of the transition-state will provide valuable information to predict cyclization trends. Although modeling the transition-state was out of the scope of this work, a figure showing a conformational rearrangement towards the reaction transition-state is shown in the Supplementary Material section, Fig. S2.

Representative structures identified from the trajectory of peptide "**b**" are shown in Fig. 4B. Among the three peptides, cyclization in peptide "**b**" was minor. Indeed, the relative energies showed the extended conformation as the most stable, Table 3. It is worth noting that "curved" structures were also sampled. Nonetheless, their relative energies were appreciably higher than the lowest energy structure, which may explain the poor cyclization tendencies of this peptide. In peptide "**c**" the most stable conformer corresponded to an "extended" structure, Fig. 4C. It seems likely that lower energy conformers with "curved" structures may be sampled in a more exhaustive conformational searching simulation. As a premise,

Table 3 Energies for representative structures from clusters and for all structures in clusters identified during the MD simulation

Cluster representative	B3LYP/PCM/cc-pVTZ//HF/6-31G*[a]	Relative energy[b] (B3LYP)	Average energy[b] (NAMD)	Relative energy[b] (NAMD)	Inter-terminal distance (Å)
Peptide "a"					
Cluster1	−2,520.0061000	8.13	94.81 ± 9.05	3.33	7.56 ± 1.10
Cluster2	−2,520.0127305	3.97	102.44 ± 9.80	10.96	9.46 ± 1.89
Cluster3	−2,520.0166828	1.49	101.43 ± 8.16	9.95	6.93 ± 2.15
Cluster4	−2,520.0156709	2.12	100.38 ± 9.95	8.90	4.94 ± 0.55
Cluster5	−2,520.0177185	**0.84**	102.13 ± 8.13	10.65	11.645 ± 1.41
Cluster6	−2,520.0190505	**0.00**	91.48 ± 8.73	**0.00**	4.75 ± 0.51
Cluster7	−2,520.0142891	2.99	95.57 ± 7.00	4.09	11.01 ± 0.35
Cluster8	−2,520.0105646	5.32	109.49	18.01	8.53 ± 0.35
Peptide "b"					
Cluster1	−2,520.0153052	6.61	92.28 ± 8.45	**0.75**	7.03 ± 1.66
Cluster2	−2,520.0227110	1.96	97.70 ± 8.77	6.17	12.39 ± 0.81
Cluster3	−2,520.0258413	**0.00**	97.17 ± 6.45	5.64	10.42 ± 0.86
Cluster4	−2,520.0211452	2.95	91.53 ± 7.07	**0.00**	4.45 ± 1.00
Cluster5	−2,520.0161913	6.06	109.07 ± 18.43	17.54	12.40 ± 0.65
Peptide "c"					
Cluster1	−2,520.0137990	6.94	94.31 ± 8.59	**0.00**	11.07 ± 1.11
Cluster2	−2,520.0227255	1.33	102.00 ± 10.39	7.69	9.29 ± 1.26
Cluster3	−2,520.0180482	4.27	96.16 ± 7.69	1.85	11.02 ± 1.76
Cluster4	−2,520.0119503	8.10	98.84 ± 5.96	4.53	6.58 ± 1.25
Cluster5	−2,520.0248523	**0.00**	96.50 ± 6.94	2.19	13.17 ± 0.69

[a] Hartrees, 1 Hartree ~627.5 kcal/mol

[b] Kcal/mol

The B3LYP and NAMD energies were computed from representative structures from clusters from all the structures in a given cluster, respectively. The lowest energies are shown in bold

conformers of peptide "**c**" with ψ_1 values between 60 and 150° coupled with (φ_3, ψ_3) values of (30–90°, 120°) in the α_L region of the Ramachandran plot, could potentially bring the *N*- and *C*-terminals in closer proximity for the peptide to undergo cyclization. In terms of the cyclization propensities, the MM energies were consistent with peptide "**a**" wherein a cluster of "curved" structures was predicted to be the most stable. On the other hand, "curved" and "extended" structures were the most stable for peptides "**b**" and "**c**," respectively, in disagreement with the cyclization tendencies. The QM energies predicted correctly the reactivities of peptides "**a**" and "**b**," but not "**c**."

Alternative starting structures for peptides "b" and "c"

The absence of low-energy pseudo-cyclic or "curved" backbone topologies in peptide "**c**" during the MD simulation may also be due to the unobserved sampling of (φ, ψ) rotamers of D-Leu2 and D-Phe4 in the experimentally most populated well of the Ramachandran diagram centered approximately at (120°, −135°). Indeed, it was possible to construct another pseudo-cyclic model of peptide "**c**" employing (φ, ψ) values of (120°, −135°) for D-Leu2 and D-Phe4, and (−87°, 129°) for Thr3. The values for Thr3 were the averages sampled during the MD simulation. When the (φ, ψ) values of (120°, −135°) for D-Phe4 were incorporated in peptide "**b**" a pseudo-cyclic backbone structure was not generated. However, for completeness another pair of 20-ns MD simulations at 310 K was performed with peptide "**c**" starting from the constructed "curved" backbone topology, and with peptide "**b**" employing initial (φ, ψ) values of (120°, −135°) for D-Phe4. The (φ, ψ) rotamers of both peptides populated during the simulations are shown in Fig. 5.

In peptide "**b**" the main differences between this simulation and the previous simulation reside in the backbone rotamers of residues Leu2 and Thr3, Fig. 5A. During the first seven nanoseconds the Leu2 sampled (φ, ψ) values of (61 ± 11.0°, 48 ± 16.6°) which were not observed in the previous simulation. After this time period these rotamers underwent transitions to values similar to those in the previous simulation. Noteworthy, these transitions occurred concurrently with a switch of the ψ angle of Thr3 from −26 ± 15.8° to 135 ± 16.1°. The latter rotamer was not

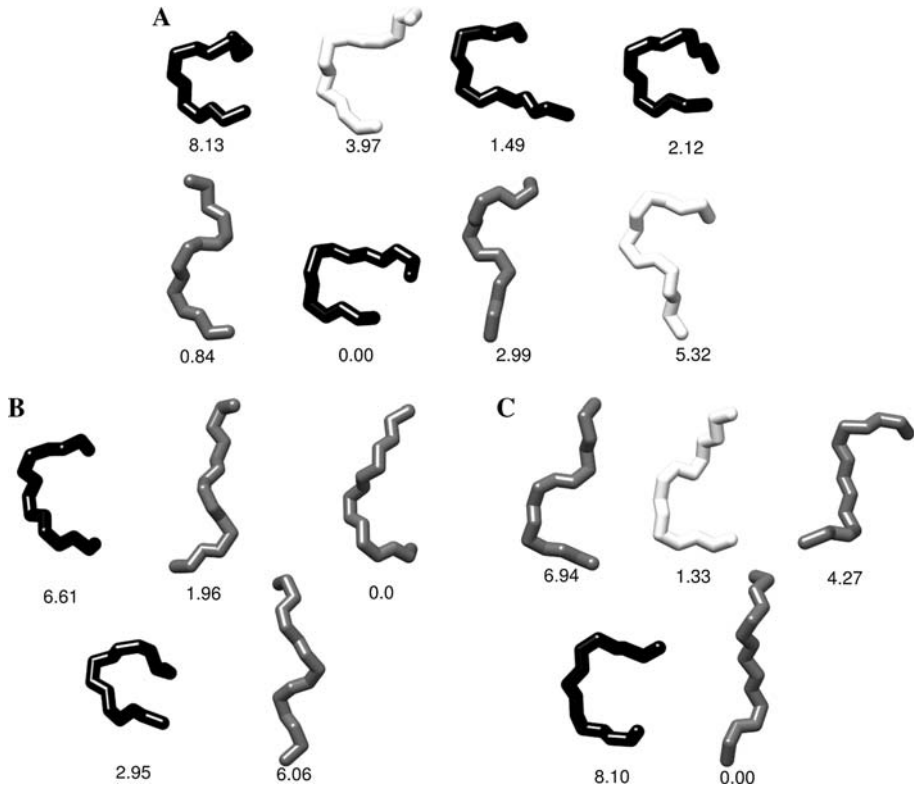

Fig. 4 Backbone conformations of representative structures from clusters identified in the 20-ns trajectories of peptides "**a**", "**b**", and "**c**" **A**, **B**, and **C**, respectively. Relative energies computed at B3LYP/cc-pVTZ level of theory with the PCM solvation model are shown. *Black*: *curved*; *white*: transition (neither *curved* nor extended); *gray*: extended

populated in the previous simulation with "**b**." In addition, the (φ_2, ψ_2) and ψ_3 transitions coincided with the formation of an unstable Leu2 O–Gly NH5 hydrogen bond interaction, Fig. 6A.

It should be noted that after the flip φ_2 and ψ_3 remained in their respective rotamers. The determinant of this stability is unclear. However, given the on-off nature of this hydrogen bond insufficient sampling may be attributed to the persistence of the latter (φ_2, ψ_3) rotamers. In the simulation with peptide "**c**" the (φ_3, ψ_3) rotamers of Thr3 adopted values of ($-88 \pm 25.5°$, $131 \pm 17.2°$) during the first 12 ns, which were similar to those sampled in the previous simulation, ($-87 \pm 29.4°$, $129 \pm 19.9°$). After 12 ns an additional set of (φ_3, ψ_3) rotamers with values of ($-136 \pm 31.3°$, $159 \pm 14.0°$) was populated, Fig. 5B. Closer examination revealed that the latter rotamers were stabilized by a hydrogen bond interaction between the Thr3 side chain oxygen atom (OG1) and the Phe4 backbone amide hydrogen atom (HN). The formation of this hydrogen bond in turn depended on the χ_1 rotamers of Thr3, Fig. 6B. Notably, the interaction was absent over the course of the first 12 ns when the χ_1 angle adopted ± *gauche* rotamers of $53 \pm 10.3°$ and $-55 \pm 10.3°$ with corresponding hydrogen bond distances of 4.1 ± 0.3 Å and 4.6 ± 0.1 Å, respectively. On the other hand, the hydrogen bond interaction distance persisted, with a value of 3.1 ± 0.1 Å, when the χ_1 angle existed in the *anti* rotamer $-168 \pm 9.3°$. This represents a scenario wherein a side chain influences the backbone conformation of a peptide.

Interestingly, during the equilibration stages of both simulations the (φ, ψ) dihedral angles of all the D-residues flipped from the initial (120°, −135°) values to the (+*gauche*, +*gauche*) rotamers as observed in the previous simulations, Fig. 5. The consistent occupation of the α_L quadrant by the D-Leu2 and D-Phe4 amino acids may point to a need for further refinement of the force field to describe D-amino acids more accurately. Nevertheless, the trajectories were clustered and the relative energies of representative structures from each cluster were determined at the B3LYP/PCM/cc-pVTZ//HF/6-31G* level of theory, Table 4, Fig. 7A, B.

In peptide "**b**" all three classes of backbone topologies were populated, while only the "transition" and "extended" topologies were observed in peptide "**c**." The MM analyses incorrectly identified "curved" and "extended" conformers as the most stable for peptides "b" and "c," respectively. Nonetheless, the QM results were more consistent with the experimental data, predicting an "extended" backbone topology as the most stable for "**b**," with a "curved" structure lying closely at 0.12 kcal/mol. For "**c**" an "extended" structure emerged once more as the most stable, in contrast to the experimental data. It is possible that at 310 K and in the 20-ns time frame peptide "**c**" does not undergo wide sampling.

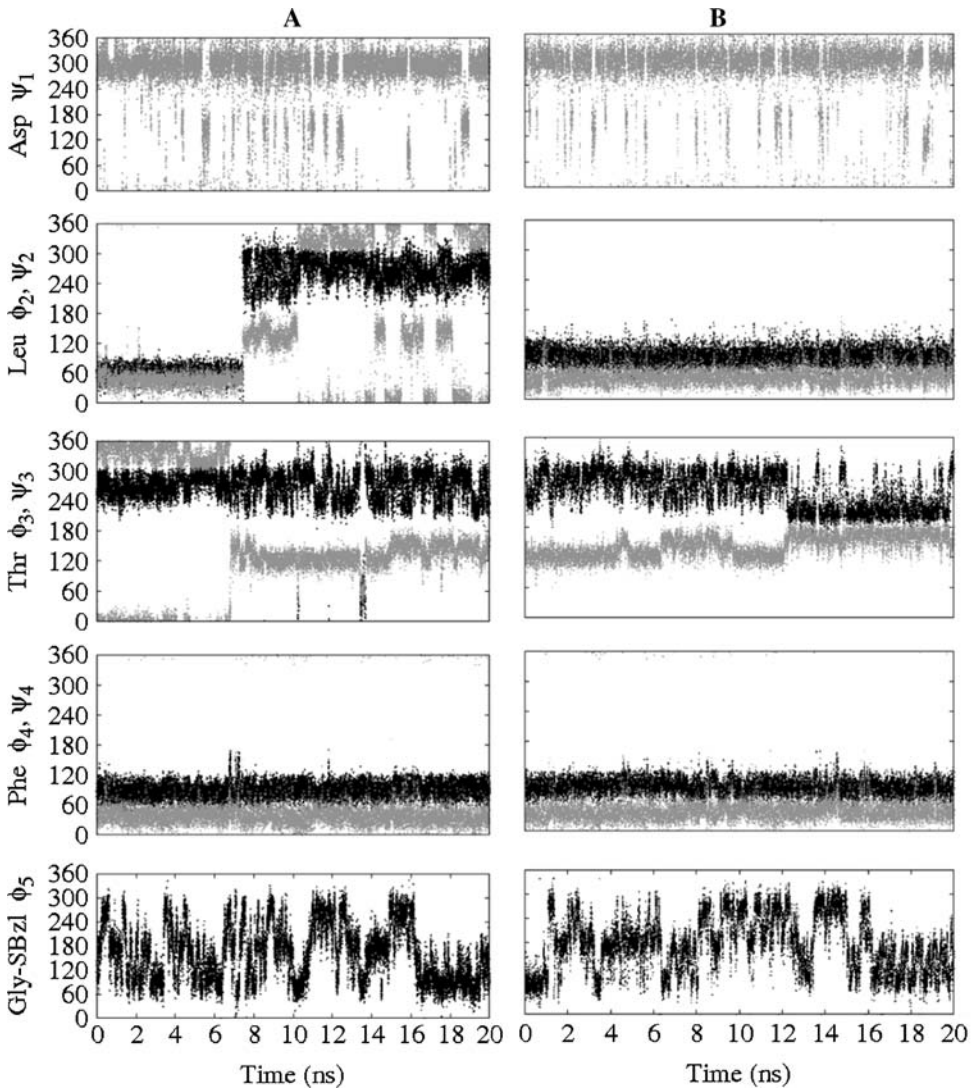

Fig. 5 The (φ, ψ) trajectories during the simulation of peptides "**b**" and "**c**," performed at 310 K starting from the experimentally predominant (φ, ψ) rotamers (120°, −135°) of the D-amino acids: D-Leu2 and D-Phe4. *A*: peptide "**b**;" *B*: peptide "**c**." φ = *black*; ψ = *gray*

Enhanced sampling for peptide "c"

Therefore, another 20-ns explicit solvent MD simulation was performed at 750 K under constant volume, to enhance conformational sampling in peptide "**c**." The trajectory was clustered and the relative energies of the representative structures from the clusters were computed at the B3LYP/PCM/cc-pVTZ//HF/6-31G* level of theory. The (φ, ψ) rotamers populated in the course of the simulation are shown in Fig. 8.

The effects of the high temperature are evident when the sampled rotamers are compared with those at 310 K: the terminal residues and Thr3 clearly populated additional rotamers. Interestingly, even at 750 K the (φ, ψ) angles of D-Leu4 and D-Phe4 predominantly sampled only their respective +*gauche* rotamers. Once more, the (φ, ψ) rotamers of Thr3 resulted in a predominance of a β-turn local conformation. However, unlike at 310 K, φ-values of Thr3 in the +*gauche* rotamer were sampled in the latter parts of the simulation, albeit fleetingly, Fig. 8. These +*gauche* φ-rotamers of Thr3 coupled with their corresponding ψ-rotamers from the MD simulation gave rise to the α_L-local conformation of Thr3 crucial for the cyclization of peptide "**c**". The relative energies and representative structures of each cluster are presented as Fig. S1 and Table S1 in the Supplementary material section. Even at this high temperature, a structure with an extended backbone topology was predicted as the most stable.

Conclusions

Molecular dynamics simulations were performed to provide insights about the experimental cyclization propensities of diastereomeric pentapeptides: "**a**," "**b**" and "**c**." Hydrogen bonding data between residues in the (i, $i \pm 3$) and (i, $i \pm 4$) configuration indicated a significant presence of pseudo-cyclic and extended backbone topologies for

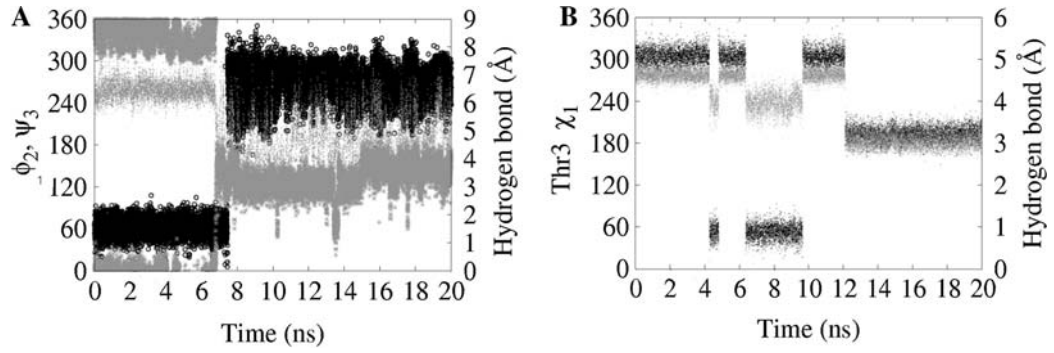

Fig. 6 Inter-dependence of hydrogen bonds and dihedral angles during the simulations "**b**" and "**c**" initiated from the experimentally most populated the (φ, ψ) rotamers (120°, −135°) of the D-amino acids: D-Leu2 and D-Phe4. *A*: φ2 (*black circles*, ●), ψ3 (*gray asterisks*, *) and Leu2 O–Gly5 NH (*gray points*); *B*: χ_1 (*black points*), Thr3 OG1–Phe4 NH (*gray points*)

Table 4 Energies for representative structures from clusters and for all structures in clusters identified during the MD simulation starting from the experimentally dominant (φ, ψ) rotamers for D-amino acids

Cluster representative	B3LYP/PCM/cc-pVTZ//HF/6-31G*[a]	Relative energy[b] (B3LYP)	Average energy[b] (NAMD)	Relative energy[b] (NAMD)	Inter-terminal distance (Å)
Peptide "b"					
Cluster1	−2,520.0152866	5.17	100.89 ± 9.06	9.78	10.17 ± 1.26
Cluster2	−2,520.0050772	11.58	100.98 ± 8.91	9.87	8.80 ± 1.54
Cluster3	−2,520.0045574	11.91	99.21 ± 9.15	8.10	8.70 ± 1.91
Cluster4	−2,520.0233358	**0.12**	100.19 ± 8.49	9.08	5.70 ± 0.89
Cluster5	−2,520.0113528	7.64	107.30 ± 7.27	16.19	11.82 ± 1.01
Cluster6	−2,520.0154512	5.07	108.00 ± 10.33	16.89	10.70 ± 2.28
Cluster7	−2,520.0180456	3.44	91.11 ± 9.01	**0.00**	5.16 ± 0.99
Cluster8	−2,520.0235325	**0.00**	104.00 ± 3.97	12.89	12.50 ± 0.54
Peptide "c"					
Cluster1	−2,520.0133286	7.11	92.70 ± 8.47	**0.03**	11.03 ± 1.09
Cluster2	−2,520.0246542	**0.00**	92.67 ± 9.08	**0.00**	12.41 ± 1.57
Cluster3	−2,520.0083969	10.20	99.05 ± 10.14	6.38	9.49 ± 1.15
Cluster4	−2,520.0209251	2.34	94.94 ± 11.09	2.27	9.13 ± 1.14
Cluster5	−2,520.0036622	13.17	98.35 ± 6.61	5.68	14.47 ± 0.22

[a] Hartrees, 1 Hartreee ~627.5 kcal/mol

[b] Kcal/mol

The B3LYP and NAMD energies were computed from representative structures from clusters from all the structures in a given cluster, respectively. The lowest energies are shown in bold

peptides "**a**" and "**b**," respectively, correctly reproducing their experimental cyclization tendencies. The hydrogen bond occupancy in peptide "**c**," although higher than that in "**b**" was still lower than expected. Similar trends were observed from the B3LYP/PCM/cc-pVTZ//HF/6-31G* relative energies of the backbone conformers within each peptide: in "**a**" the pseudo-cyclic conformer was the most stable, while in "**b**" an extended conformer was predicted to be the most stable, in agreement with the experimental data; however, in "**c**" an "extended" backbone conformer was the most stable at 310 and at 750 K. The MM-derived average energies of each cluster were consistent with only peptide "**a**." Additional simulations conducted with the initial (φ, ψ) rotamers of the D-amino acids in the experimentally predominant segment of the Ramachandran plot consistently flipped the rotamers to the experimentally less populated α_L segment. This observation suggests the need for further refinement of the force field to enhance sampling for amino acids with the D-stereochemistry. At this stage, the conformational preferences of oligopeptides consisting of all L-amino acids can be elucidated with the careful selection of a parameter set and simulation protocols. However, defining the conformational properties of peptides bearing D-amino acids is not straightforward. Continual development of current force fields is expected to provide far-reaching conformational sampling of peptides

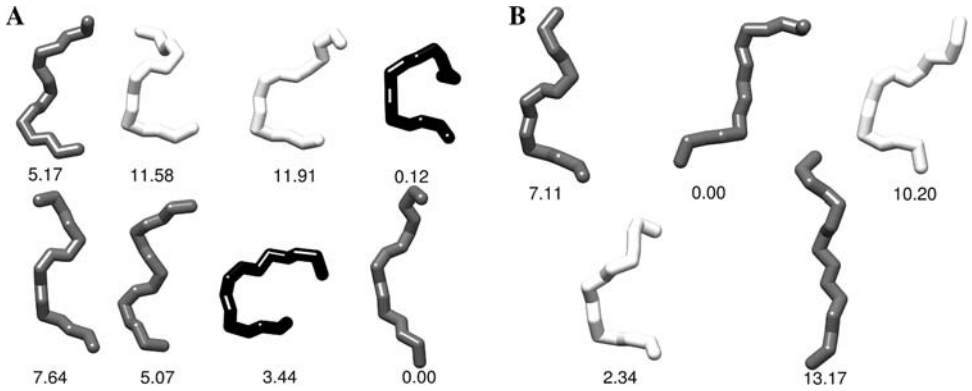

Fig. 7 Backbone conformations of representative structures from clusters identified in the 20-ns trajectories of peptides "**b**", and "**c**" **A** and **B**, respectively, with initial backbone (φ, ψ) rotamers at (120°, −135°) for the D-amino acid residues. B3LYP/PCM/cc-pVTZ relative energies are shown. *Black* curved; *white* transition (neither curved nor extended); *gray* extended

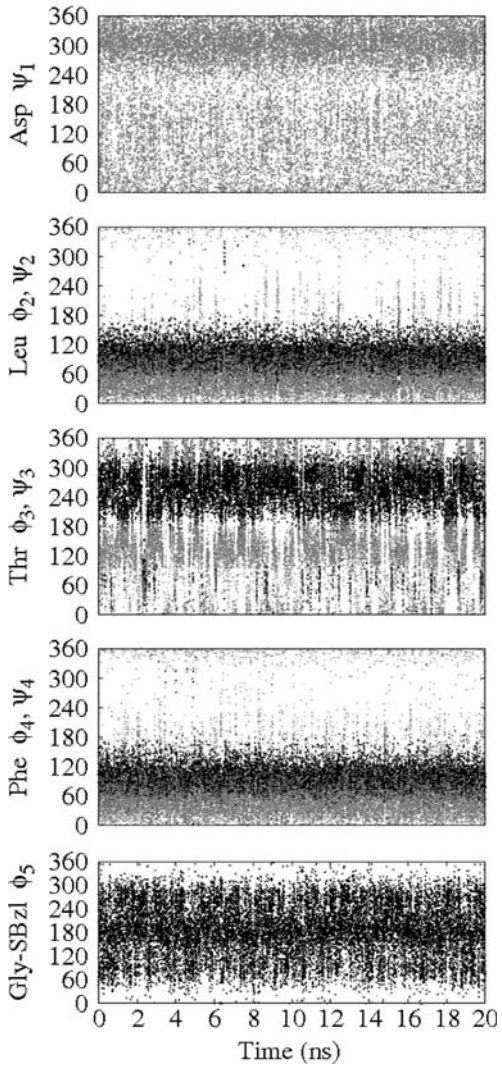

Fig. 8 The (φ, ψ) trajectories during the simulation of peptide "**c**" performed at 750 K. φ = *black* ψ = *gray*. *Note* the *black* streaks at ~60° in the Thr (φ_3, ψ_3) trajectory. φ-values at this rotamer and the corresponding ψ-values in the trajectory result in "*curved*" backbone topologies

containing D-residues. These improvements along with a characterization of the transition-states will increase the potential of employing these simulations to guide the design of cyclic peptides. Furthermore, computing time and cost of explicit-solvent MD simulations are steadily decreasing thanks to the development of high-speed computing platforms.

Acknowledgments This work was supported by the State of Florida, Executive Officer of the Governor's Office of Tourism, Trade and Economic Development, and by the National Science Foundation (CHE0455072 to R. A. H.). Authors thank the University Of Georgia Research Computing Center for supercomputing time, and the Theoretical and Computational Biophysics Group UIUC for providing VMD and NAMD programs. We are thankful to the referees for helpful criticisms of this manuscript.

References

1. Craik DJ (2006) Science 311:1563
2. Goncalves V, Gautier B, Coric P, Bouaziz S, Lenoir C, Garbay C, Vidal M, Inguimbert N (2007) J Med Chem 50:5135
3. Daly NL, Chen Y-K, Foley FM, Bansal PS, Bharathi R, Clark RJ, Sommerhoff CP, Craik DJ (2006) J Biol Chem 281:23668
4. Ireland DC, Wang CKL, Wilson JA, Gustafson KR, Craik DJ (2008) Biopolymers 90:51
5. Daly NL, Clark RJ, Plan MR, Craik DJ (2006) Biochem J 393:619
6. Horne WS, Wiethoff CM, Cui C, Wilcoxen KM, Amorin M, Ghadiri MR, Nemerow GR (2005) Bioorg Med Chem 13:5145
7. De Luca S, Saviano M, Della Moglie R, Digilio G, Bracco C, Aloj L, Tarallo L, Pedone C, Morelli G (2006) Chem Med Chem 1:997
8. Pakkala M, Hekim C, Soininen P, Leinonen J, Koistinen H, Weisell J, Stenman UH, Vepsalainen J, Narvanen A (2007) J Pept Sci 13:348
9. Sun H, Greeley DN, Chu X-J, Cheung A, Danho W, Swistok J, Wang Y, Zhao C, Chen L, Fry DC (2004) Bioorg Med Chem 12:2671
10. Korsinczky MLJ, Schirra HJ, Craik DJ (2004) Curr Protein Pept Sci 5:351

11. Dooley CT, Chung NN, Wilkes BC, Schiller PW, Bidlack JM, Pasternak GW, Houghten RA (1994) Science 266:2019
12. Houghten RA, Dooley CT, Appel JR (2006) AAPS Journal 8:E371
13. Davies JS (2003) J Pept Sci 9:471
14. Jeremic T, Linden A, Moehle K, Heimgartner H (2005) Tetrahedron 61:1871
15. Glaves R, Baer M, Schreiner E, Stoll R, Marx D (2008) Chem Phys Chem 9:2759
16. Ehrlich A, Heyne HU, Winter R, Beyermann M, Haber H, Carpino LA, Bienert M (1996) J Org Chem 61:8831
17. Mitchell JBO, Smith J (2003) Proteins Struct Funct Genet 50:563
18. Schweitzer-Stenner R, Gonzales W, Bourne GT, Feng JA, Marshall GR (2007) J Am Chem Soc 129:13095
19. Terada T, Satoh D, Mikawa T, Ito Y, Shimizu K (2008) Proteins Struct Funct Bioinf 73:621
20. Krautler V, Aemissegger A, Hunenberger PH, Hilvert D, Hansson T, van Gunsteren WF (2005) J Am Chem Soc 127:4935
21. Bozzi A, Di Giulio A, Aschi M, Rinaldi AC (2008) J Pept Sci 14:769
22. Beck DAC, White GWN, Daggett V (2007) J Struct Biol 157:514
23. Galzitskaya OV, Higo J, Finkelstein AV (2002) Curr Protein Pept Sci 3:191
24. Cavelier-Frontin F, Pepe G, Verducci J, Siri D, Jacquier R (1992) J Am Chem Soc 114:8885
25. Besser D, Olender R, Rosenfeld R, Arad O, Reissmann S (2000) J Pept Res 56:337
26. Seibert MM, Patriksson A, Hess B, van der Spoel D (2005) J Mol Biol 354:173
27. Pettersen EF, Goddard TD, Huang CC, Couch GS, Greenblatt DM, Meng EC, Ferrin TE (2004) J Comput Chem 25:1605
28. Mackerell ADJ, Feig M, Brooks CLI (2004) J Comput Chem 25:1400
29. Humphrey W, Dalke A, Schulten K (1996) J Mol Graphics 14:27
30. Jorgensen WL, Swenson CJ (1985) J Am Chem Soc 107:569
31. Phillips JC, Braun R, Wang W, Gumbart J, Tajkhorshid E, Villa E, Chipot C, Skeel RD, Kale LV, Schulten K (2005) J Comput Chem 26:1781
32. Darden T, York D, Pederson L (1993) J Chem Phys 98:10089
33. Hess B, Kutzner C, van der Spoel D, Lindahl E (2008) J Chem Theory Comput 4:435
34. Barone V, Cossi M, Tomasi J (1998) J Comput Chem 19:404
35. Frisch MJ, Trucks GW, Schlegel HB, Scuseria GE, Robb MA, Cheeseman JR, Montgomery Jr JA, Vreven T, Kudin KN, Burant JC, Millam JM, Iyengar SS, Tomasi J, Barone V, Mennucci B,Cossi M, Scalmani G, Rega N, Petersson GA, Nakatsuji H, Hada M, Ehara M, Toyota K, Fukuda R, Hasegawa J, Ishida M, Nakajima T, Honda J, Kitao O, Nakai H, Klene M, Li X, Knox JE, Hratchian HP, Cross JB, Adamo C, Jaramillo J, Gomperts R, Stratmann RE,Yazyev O, Austin AJ, Cammi R, Pomelli C, Ochterski JW, Ayala PY, Morokuma K, Voth GA, Salvador P, Dannenberg JJ, Zakrzewski VG, Dapprich S, Daniels AD, Strain MC, Farkas O, Malick DK, Rabuck AD, Raghavachari K, Foresman JB, Ortiz JV, Cui A, Baboul AG, Clifford S, Cioslowshi J, Stefanov BB, Liu G, Liashenko A, Piskorz P, Komaromi I, Martin RL, Fox DJ, Keith T, Al-Laham MA, Peng CY, Nanayakkara A, Challacombe M, Gill PMW, Johnson B, Chen W, Wong MW, Gonzalez C, Pople JA (2004) In: Gaussian, Inc, Wallingford, CT
36. Li Y, Yu Y, Giulianotti M, Houghten RA (2008) J Comb Chem 10:613
37. Li Y, Yongye A, Giulianotti M, Martinez-Mayorga K, Yu Y, Houghten R (2009) J Comb Chem (submitted)
38. Schmidt U, Langner J (1997) J Pept Res 49:67
39. Chen Y, Mant CT, Hodges RS (2002) J Pept Res 59:18
40. Durani S (2008) Acc Chem Res 41:1301
41. Avbelj F, Moult J (1995) Biochemistry 34:755
42. Mathews CK, van Holde EK, Ahern KG (2000) Biochemistry. Pearson Prentice Hall, USA